## Cluster tomography in percolation

Helen S. Ansell , <sup>1,2</sup> Samuel J. Frank , <sup>1,3</sup> and István A. Kovács <sup>1,4,5,\*</sup>

<sup>1</sup>Department of Physics and Astronomy, Northwestern University, Evanston, Illinois 60208, USA

<sup>2</sup>Department of Physics, Emory University, Atlanta, Georgia 30322, USA

<sup>3</sup>Department of Physics, Northeastern University, Boston, Massachusetts 02115, USA

<sup>4</sup>Northwestern Institute on Complex Systems, Northwestern University, Evanston, Illinois 60208, USA

<sup>5</sup>Department of Engineering Sciences and Applied Mathematics, Northwestern University, Evanston, Illinois 60208, USA

(Received 26 July 2023; accepted 9 November 2023; published 8 December 2023)

In cluster tomography, we propose measuring the number of clusters N intersected by a line segment of length  $\ell$  across a finite sample. As expected, the leading order of  $N(\ell)$  scales as  $a\ell$ , where a depends on microscopic details of the system. However, at criticality, there is often an additional nonlinearity of the form  $b \ln(\ell)$ , originating from the endpoints of the line segment. By performing large scale Monte Carlo simulations of both two- and three-dimensional percolation, we find that b is universal and depends only on the angles encountered at the endpoints of the line segment intersecting the sample. Our findings are further supported by analytic arguments in two dimensions, building on results in conformal field theory. Being broadly applicable, cluster tomography can be an efficient tool for detecting phase transitions and characterizing the corresponding universality class in classical or quantum systems with a relevant cluster structure.

DOI: 10.1103/PhysRevResearch.5.043218

#### I. INTRODUCTION

Cluster formation is a prevalent feature of complex systems, including but not restricted to magnetic domains [1], motility-induced phase separation [2–4], bacteria swarming [5], cell migration [6,7] and the collective motion of animal groups [8-11]. As phase transitions often lead to changes in the characteristics of the emerging clusters, phase transitions can-in principle-be detected and studied through cluster statistics. As a realization, let us consider a scenario where a probe is shot through a complex system consisting of clusters and ask the following question: How many clusters are encountered by the probe during the measurement? Here we propose that such measures of "cluster tomography" yield simple and efficient methods for locating critical points in a broad range of complex systems, both experimentally and computationally, while also providing deep universal information on the nature of the observed transitions.

Motivated by questions on quantum entanglement in disordered systems [12–14], previous studies have considered the number of clusters (magnetic domains),  $N_{\Gamma}$ , intersecting a contour,  $\Gamma$ , focusing on a few select geometries. Cluster tomography corresponds to the simplest case of skeletal entanglement [15] when  $\Gamma$  is a line segment. For select line

Published by the American Physical Society under the terms of the Creative Commons Attribution 4.0 International license. Further distribution of this work must maintain attribution to the author(s) and the published article's title, journal citation, and DOI.

configurations of length  $\ell$ , it was found that at criticality

$$N(\ell) = a\ell + b\ln(\ell) + O(1),\tag{1}$$

in both two and three dimensions (2d and 3d) [12,13,16,17]. The first term represents the expected "area law" scaling of the number of clusters with the length of the line, with a being the nonuniversal linear cluster density. The subleading term  $b \ln(\ell)$  is known as the "corner contribution," which emerges due to the geometric singularities at the endpoints of the line segment, akin to a notion of "geometric susceptibility" [18]. This term is present only at criticality and is an elegant measure of the concavity of the underlying cluster geometry that encapsulates universal information from correlations in the cluster shape at all orders, as discussed further in Appendix B.

Here, as an illustration of cluster tomography, we systematically address all ten possible line configurations in a 2d square system [illustrated in Fig. 1(a)]. We focus on Bernoulli percolation on a square lattice, although the main results are expected to apply more generally [14] for any system with a relevant cluster structure. We present analytic results in 2d backed up by high-precision numerics for the corner contribution of all previously unstudied line segment types (lines 3–10) for critical site and bond percolation on a square lattice. With the developed high precision numerical techniques we demonstrate that the corner contribution term is present in all of these line segment configurations. The corresponding "cluster count exponent" b is found to be universal, with dependence on the configurations of the line segment endpoints. In addition, we consider select line configurations in a 3d cubic system, where only the bulk line has been studied [16]. While there are no analytic predictions for line segments in 3d, we numerically show that, as in 2d, the corner contribution of line segments that pass through the bulk is logarithmic, with a

<sup>\*</sup>istvan.kovacs@northwestern.edu

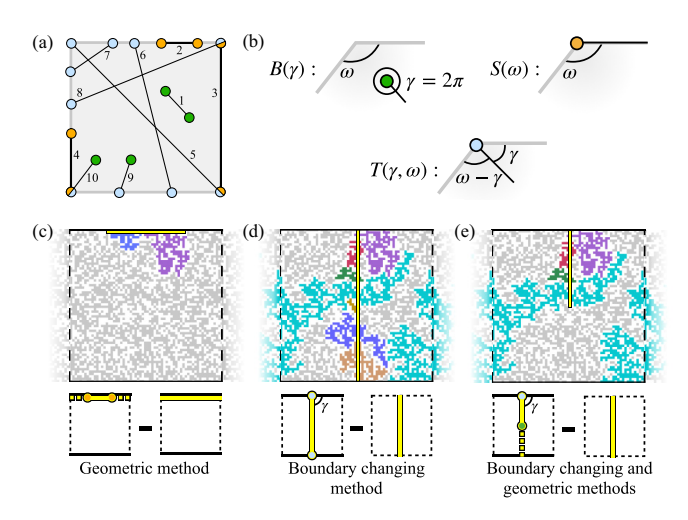


FIG. 1. (a) Summary of all line segment types in a 2d square system with free boundaries. Endpoints of the lines are colored according to the classification in (b): bulk (green), surface (orange), and traversing (blue). (c)–(e) Schematics of contributing clusters and numerical techniques used to access the critical corner contribution of different line segments for site percolation, illustrated for line types 2, 6, and 9. Dashed black lines represent periodic boundary conditions (PBC), solid lines represent free boundary conditions (FBC), and solid yellow lines represent the measured line segment. Sites belonging to clusters that are counted by the line segment are colored while the remaining occupied sites are gray.

universal b that depends on the endpoint configurations. However, unlike in 2d, we find that the line segments contained entirely within a surface of the system yield b=0.

More generally, cluster tomography provides an efficient way of detecting phase transitions in clustered systems by tuning the control parameter and looking for the presence of a corner contribution term. We demonstrate this conceptually for percolation, showing how cluster tomography can be used to both locate the critical point, and determine critical exponents.

# II. ANALYTIC RESULTS FOR THE CORNER CONTRIBUTION IN 2d

We first develop analytic predictions for the corner contribution of each line segment type in Fig. 1(a) for critical percolation. Percolation is a fundamental model of critical phenomena, where sites or bonds of a lattice are independently occupied with probability p. Collective behavior emerges as we are interested in the statistics of clusters of connected sites [19]. In dimensions  $d \ge 2$  there is a scale-invariant critical point at  $p = p_c$  at which the system is also believed to be conformally invariant [20]. In the most studied 2d case, there are many exact results available [21–24], including correlation functions [25], crossing probabilities [26], and critical exponents.

In cluster tomography, we expect that the "cluster count exponent" b is universal for a given line configuration. That is, b is independent of the microscopic details of the model at criticality. For sufficiently long lines—i.e.,  $\ell/L = O(1)$ , with L being the system size—each endpoint is expected to

contribute to b independently. We conjecture that the contribution of each endpoint depends on its topology and the angles encountered by the endpoint, with three distinct cases in 2d: bulk b, surface s, and traversing t, as illustrated in Fig. 1(b). Bulk endpoints occur when the endpoint is not on the surface, and have a characteristic angle  $\gamma = 2\pi$ . Surface endpoints, for which the corner contribution depends on the angle  $\omega$  of the boundary at the endpoint, occur when the line segment is along the surface. Traversing endpoints occur when the line segment crosses the bulk of the system and has its endpoint on the surface. In this case, the corner contribution depends on both  $\omega$  and the angle  $\gamma$  between the line segment and the boundary. For line types 1–5 this means that the value of b is expected to be universal, while for lines 6–10 b is expected to be a universal function of the characteristic angle  $\gamma$ .

Supported by analytic arguments from conformal field theory (see Appendix A for details), we expect that the contributions of the endpoints consist of linear combinations of a bulk term *B* and a surface term *S*, depending on the configuration. The bulk term

$$B(\gamma) = \frac{5\sqrt{3}}{96\pi} \left( \frac{\gamma}{\pi} - \frac{\pi}{\gamma} \right) \tag{2}$$

follows from the celebrated Cardy-Peschel formula [27]. This appears for endpoints in the bulk, with each contributing  $B(2\pi)$  to b. Note that for contours with angles  $0 < \gamma < 2\pi$ , the bulk corner contribution would be the sum of  $B(\gamma)$  and the conjugate angle  $B(2\pi - \gamma)$  [13,14]. However, for  $\gamma = 2\pi$ , the contribution is just  $B(2\pi)$ , as the singular B(0) is not sampled by the measurement [13,14].

We conjecture that the surface term

$$S(\gamma) = \frac{\sqrt{3}}{8\pi} \frac{\pi}{\gamma} \tag{3}$$

appears whenever there is a change of boundary condition at the endpoint [28,29]. Such a change of boundary condition occurs when the line segment along which clusters are counted (fixed boundary) meets the surface (free boundary) at an angle, which occurs for type s and t endpoints. Surface endpoints each contribute  $S(\omega)$  to b. For line 2, this has been shown numerically on the square lattice [13], and proven rigorously on the triangular lattice [30].

Traversing endpoints are more complicated, as multiple angles contribute. These line segments pass through the bulk and end on the surface, forming angles  $\gamma$  and  $\omega - \gamma$  with the free system boundary, as illustrated in Fig. 1(b). Given that the line segment crosses the bulk, we expect bulk contributions  $B(\gamma)$  and  $B(\omega - \gamma)$  from the two angles. Additionally, the change in boundary conditions from fixed to free at the endpoint results in  $S(\gamma)$  and  $S(\omega - \gamma)$  terms contributing. However, naively taking the sum of these four terms gives the contribution from jointly counting clusters along the free boundary in addition to the line segment of interest, as illustrated in Fig. S1 of the Supplemental Material [31]. The contribution of the additional clusters counted is equivalent to counting along a contour that follows the edge of the system and has angle  $\omega$ . Subtracting the contribution  $B(\omega)$  of this contour therefore

TABLE I. Overview of results for 2d percolation on a square lattice. Analytic and numerical values are given for the least acute angle studied  $\gamma(n_{\min})$  in cases where b depends on  $\gamma$ . Parentheses by measured values give the measurement error in the last digit. "G" and "BC" respectively refer to the geometric and boundary changing methods, \* indicates cancellation of lines of type 6 and/or 9 is required to determine b to high precision numerically. Note that for line 8 there are two equivalent expressions for the formula, depending on which endpoint is chosen to define  $\gamma$ . The expression given here uses the angle indicated in the schematic figure as  $\gamma$ .

Line	Endpoints <sup>a</sup>	Figure	Formula	$\gamma(n_{\min})$	b expected	b measured	Technique
1	bb	1	$2B(2\pi)$		$\frac{5\sqrt{3}}{32\pi} \approx 0.086^{\mathrm{b}}$	0.086(1) <sup>b</sup>	G
2	SS	•••	$2S(\pi)$		$\frac{\sqrt{3}}{4\pi} pprox 0.138^{\rm c}$	0.138(3) <sup>d</sup>	G
3	$S_c S_c$		$2S(\frac{\pi}{2})$		$\frac{\sqrt{3}}{2\pi} \approx 0.276$	0.27(2)	ВС
4	$SS_C$		$S(\pi) + S(\frac{\pi}{2})$		$\frac{3\sqrt{3}}{8\pi} pprox 0.207$	0.21(1)	G & BC
5	$t_c t_c$		$2T(\frac{\pi}{4},\frac{\pi}{2})$		$\frac{11\sqrt{3}}{8\pi} pprox 0.758$	0.76(3)	ВС
6	tt		$2T(\gamma,\pi)$	$\frac{\pi}{2}$	$\frac{11\sqrt{3}}{16\pi} \approx 0.379$	0.38(1)	ВС
7	tt'		$T(\gamma,\pi) + T(\frac{\pi}{2} - \gamma,\pi)$	$\frac{\pi}{4}$	$\frac{127\sqrt{3}}{144\pi}\approx 0.486$	0.48(2)	BC*
8	$tt_c$		$T(\gamma, \frac{\pi}{2}) + T(\frac{\pi}{2} - \gamma, \pi)$	$\arctan\left(\frac{1}{2}\right)$	$\approx 0.649$	0.66(3)	BC*
9	tb	1	$T(\gamma,\pi) + B(2\pi)$	$\frac{\pi}{2}$	$\frac{27\sqrt{3}}{64\pi} \approx 0.233$	0.24(1)	G & BC
10	$t_c b$	p	$T(\gamma, \frac{\pi}{2}) + B(2\pi)$	$\frac{\pi}{4}$	$\frac{49\sqrt{3}}{64\pi} \approx 0.422$	0.42(2)	G & BC*

a(') for line 7 indicates endpoints are on adjacent edges.

gives the contribution from the traversing endpoint,

$$T(\gamma,\omega) = B(\gamma) + S(\gamma) + B(\omega - \gamma) + S(\omega - \gamma) - B(\omega). \tag{4}$$

Note that since  $B(\pi) = 0$ , here the  $-B(\omega)$  contribution to  $T(\gamma, \omega)$  can only be detected if the traversing endpoint is in the square corner  $(\omega = \pi/2)$ . Once again,  $\gamma = 0$  requires special care, as  $T(0, \omega)$  has unmeasured singular contributions, so  $S(\omega)$  should be used directly in this case. These arguments lead to our systematically predicted expressions for the cluster count exponent  $b_{ij}$  listed in Table I, where  $i, j \in \{b, s, t\}$  denotes the endpoint type, and an additional subscript c is used on s and t in cases where the endpoint is in the corner of the square system.

# III. NUMERICAL VERIFICATION OF THE CORNER CONTRIBUTION IN 2d

The analytic predictions for 2d percolation need to be tested numerically. Moreover, in other systems lacking detailed analytic results, numerical measurements are the only option for performing cluster tomography. It is, however, not immediately obvious that the universal logarithmic corner contribution can be measured to high precision. In practice, there are multiple difficulties to overcome, including the fact that the linear term  $a\ell$  is much larger than the nonlinear term  $b\ln(\ell)$ , large statistical noise in the overall measurement  $\sim O(\sqrt{\ell})$ , and potentially strong finite-size corrections to the linear term. Strikingly, the area law term can be canceled out *exactly* together with its statistical error and finite-size

corrections, leading to precise measurements of the corner term even in relatively small systems.

For line types 1 and 2, the corner contribution can be precisely measured using a geometric method [13,16], as illustrated in Fig. 1(c) for a line segment of length  $\ell = L/2$ on a free surface with periodic boundary conditions (PBC) on the other sides of the square. The difference between the total number of clusters on two contributing segments of length  $\ell = L/2$  that together span the system and the number of clusters on a full periodic line of length L (without any endpoints) through the same lattice sites gives twice the corner contribution of the line segment. As the same sites are visited in both cases, the linear area law term cancels out and the only remaining contribution must come from the endpoints. The corner contribution  $\Delta N$  is therefore simply half the number of shared clusters between the two line segments. This approach has previously been used to numerically calculate  $b_{ss}$  in 2d (line 2), as well as  $b_{bb}$  in 2d (line 1) and 3d [13,16] for a line segment in the bulk using PBC all around. These 2d results are consistent with analytic predictions [13,30].

As the applicability of the geometric method alone is limited to these two cases, here we propose a boundary changing method to measure the corner contribution of the remaining line types with high precision. This method is expected to be applicable for cluster-based systems with short-range interactions, and is illustrated in Fig. 1(d) for a line segment with traversing endpoints on opposite sides of the system. By changing the free boundary conditions (FBC) into PBC, the same line now forms a closed loop with no endpoints. The area law term can be canceled by taking the difference  $\Delta N$  between the number of clusters that intersect the line segment

<sup>&</sup>lt;sup>b</sup>Reference [13].

<sup>&</sup>lt;sup>c</sup>References [12,13,30,32].

<sup>&</sup>lt;sup>d</sup>Reference [14].

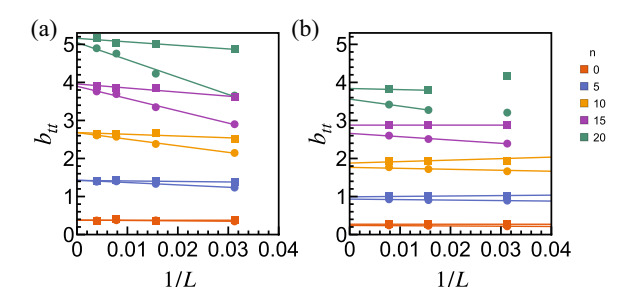


FIG. 2. Extrapolation of the cluster count exponent  $b_{tt}$  for angles  $\gamma = \arctan{(1/n)}$  for a line segment spanning the entire system (Fig. 1, line 6). As an illustration of universality, the results are shown for both site (circles) and bond (squares) percolation in (a) 2d and (b) 3d. Error bars, representing the standard error on each point, are smaller than the point marker size.

with FBC and PBC. The boundary changing method can be used alone, or in conjunction with the geometric method [as illustrated in Fig. 1(e)], to numerically determine the corner contributions of line types 3–10, including the angle dependence of lines 6–10, as indicated in Table I.

In our large-scale Monte Carlo calculations, we investigate cluster tomography for critical site and bond percolation on the simple cubic lattice in 2d and 3d. The respective critical occupancies for site and bond percolation are  $p_c$  = 0.592746 and  $p_c = 0.5$  in 2d [19] and  $p_c = 0.311608$  and  $p_c = 0.2488126$  in 3d [33,34]. We studied systems up to linear size L = 512 in 2d and L = 256 in 3d, with at least 10 000 samples in each case. For each line configuration, we calculate finite-size estimates of b(L) through two-point fits at sizes L and 2L. We then estimate b using a linear extrapolation of the largest sizes against 1/L, as shown in Fig. 2 for a line segment spanning the entire system (line 6) in 2d and 3d. The extrapolated b values for site and bond percolation agree within the error, indicating universality. Therefore, all quoted numerical b values are averaged for site and bond percolation.

In a 2d square system, line types 1–5 each have universal b values with no angle dependence. Numerical estimates for lines 3–5 are listed in Table I along with known results for lines 1-2 [12–14,30,32]. The angle dependence of lines 6-10can be explored to high precision for angles  $\gamma = \arctan(1/n)$ for integer  $n_{\min} \leqslant n \leqslant 20$ , where  $n_{\min} \to 0$  for lines 6 and 9,  $n_{\min} = 1$  for lines 7 and 10, and  $n_{\min} = 2$  for line 8. For line 6, we can directly access the  $\gamma$  dependence of b to high precision using the boundary changing method by starting with FBC on one opposite pair of system edges and PBC on the other. This approach can be used in conjunction with the geometric method for line 9. For lines 7, 8, and 10, the initial configuration must have FBC on all sides. In these cases, b values can be determined numerically to high precision by incorporating lines of type 6 and 9 into the initial configuration so that a closed loop forms after applying PBC, then subtracting their contribution from the count to determine the corner contribution of interest; see Fig. S2 of the Supplemental Material [31]. Numerical results for lines 6–10 are plotted in Figs. 3(a) and 3(b), along with the predicted analytic form of the  $\gamma$  dependence, and numerical values for  $\gamma(n_{\min})$  for each line type are listed in Table I. In all cases,

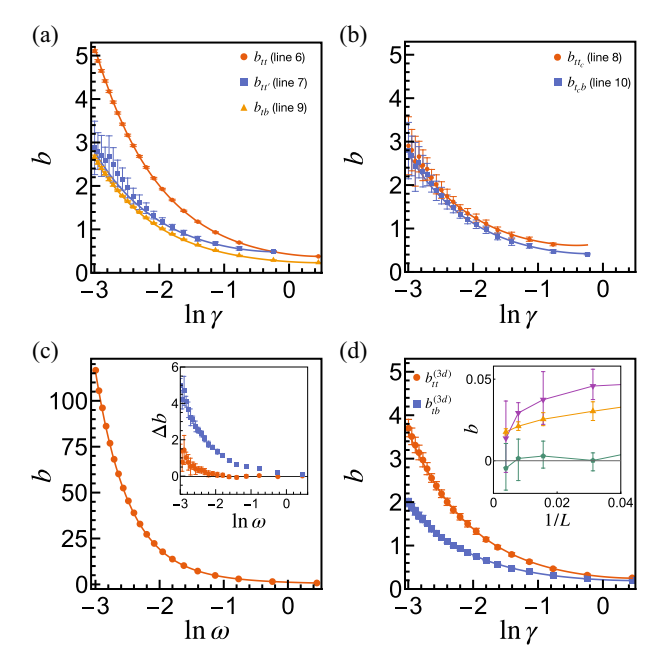


FIG. 3. (a)–(b) Angle dependence of the cluster count exponent b in 2d for lines 6–10 in Fig. 1(a). Numerically determined points and curves showing the analytic predictions given in Table I are plotted for (a)  $b_{tt}$ ,  $b_{tt'}$ , and  $b_{tb}$ , and (b)  $b_{tt_c}$  and  $b_{t_cb}$ . (c)  $b_{t_ct_c}$  (line 5) in a sheared square system with acute angle  $\omega$ . Inset: Difference  $\Delta b$  between numerical results presented in the main panel and the predicted analytic expression  $T(\gamma, \omega)$  (red circles), and the naive analytic prediction  $T(\gamma, \omega) + B(\omega)$  (blue squares). (d) Angle dependence of b in 3d for  $b_{tt}^{(3d)}$  and  $b_{tb}^{(3d)}$ . Plotted lines show a fit of the form given in Eq. (6). Inset: Estimates of b along a partial line segment on the surface of a cube (orange up triangles), a full line segment through the center of the face with  $\gamma = \pi/2$  (purple down triangles), and a full line along the edge of a cube (green pentagons) all tend to zero at large L.

we observe a good agreement between numerical values and analytic predictions.

Due to the  $-B(\omega)$  term in  $T(\gamma, \omega)$  contributing only for type  $t_c$  endpoints, we further test for the presence of this term by examining  $b_{t_ct_c}$  for line 5 as the square system is sheared with acute angle  $\omega$ . Our analytic predictions in this case give  $b_{t_c t_c} = 2T(\gamma, \omega)$  with the angle  $\gamma$  of the line across the diagonal of the sheared square system given by  $\tan(\gamma) = \tan \omega/(1 + \tan \omega)$ . Numerically, this can be tested for  $\tan \omega = 1/n$  with  $\tan \gamma = 1/(n+1)$  in a system of size L by L + n. Figure 3(c) shows numerical results for  $b_{t_ct_c}$  along with the analytic prediction. To verify that the numerical results are closer to the analytic prediction with the presence of the  $-B(\omega)$  term in  $T(\gamma, \omega)$ , we plot the difference between the numerical results and the analytic formula for  $T(\gamma, \omega)$ with and without the  $-B(\omega)$  term present in the inset of Fig. 3(c). This shows better agreement between the numerical results and analytic prediction when  $T(\gamma, \omega)$  takes the form given in Eq. (4).

### IV. CLUSTER TOMOGRAPHY IN 3d

In a 3d cubic system, there are 23 types of line segment configurations depending on whether the endpoints are touching faces, edges, corners, or the bulk, as illustrated in Fig. S3 of the Supplemental Material [31]. Of these, only the case where both endpoints of the line segment are in the bulk has been studied numerically, giving  $b_{bb}^{(3d)}=0.130(3)$  [16]. Although there are no known analytic predictions in 3d, endpoints are still expected to contribute to b independently. Therefore relations such as

$$b_{tb} = (b_{tt} + b_{bb})/2 (5)$$

will still hold true in 3d percolation and other clustered systems. We explore this relation by examining the angle dependence of a line segment spanning the cube and ending on opposite faces  $(b_{tt}^{(3d)})$ , and the case where the line segment starts on a face and ends in the bulk  $(b_{tb}^{(3d)})$ , as shown in Fig. 3(d). Motivated by the expressions for  $b_{tt}$  and  $b_{tb}$  in 2d, we fit a line of the form

$$b^{(3d)}(\gamma) = c_1 \left(\frac{\pi}{\gamma} + \frac{\pi}{\pi - \gamma}\right) + c_2,\tag{6}$$

which gives  $c_1 \sim 0.06$  and  $c_2 \sim 0.03$  for  $b_{tt}^{(3d)}$  and  $c_1 \sim 0.03$  and  $c_2 \sim 0.08$  for  $b_{tb}^{(3d)}$ . Equation (5) is satisfied within the numerical uncertainty on the data points.

At the same time, some line types might not lead to a finite *b* in 3d. In particular, the critical 3d percolation occupancy is below that in 2d at which the surface alone would lead to a logarithmic corner contribution. We investigate three cases of a line segment on a surface of the cube: a partial line segment in a face, a full line segment along an edge, and a full line segment through the center of the face parallel to an edge (lines 1, 3, and 6 in Fig. S3 of the Supplemental Material [31]). As shown in the inset of Fig. 3(d), these cases suggest that the cluster count exponent vanishes in 3d for lines fully on the surface (types 1–10 in Fig. S3 of the Supplemental Material [31]). In Appendix B and Fig. S4 of the Supplemental Material [31], we discuss how this finding is related to the shape of the clusters.

### V. USING CLUSTER TOMOGRAPHY TO LOCATE THE CRITICAL POINT AND DETECT THE UNIVERSALITY CLASS

The presence of a corner contribution term at criticality provides a simple and effective way of pinpointing the critical point and the corresponding universality class of a clustered system. As an example, Fig. 4 shows the corner contribution  $\Delta N$  for line 5 as a function of occupation probability p in 2d site percolation, using the boundary changing method. The sharp peak indicates the critical point  $p = p_c$  (dashed line), at which universal information about the system can be determined. After determining the value of  $b_{t_ct_c}$  using the methodology shown in Fig. 2, the correlation length exponent  $\nu$  can be extracted from optimal data collapse, as illustrated in Fig. 4(b).

Similar measurements could be made in a broad range of clustered systems, providing a simple, computationally efficient method for detecting the critical point as the control parameter is varied. Cluster tomography with traversing endpoints is especially promising in this regard as it leads to the strongest signals in both 2d and 3d percolation, even more

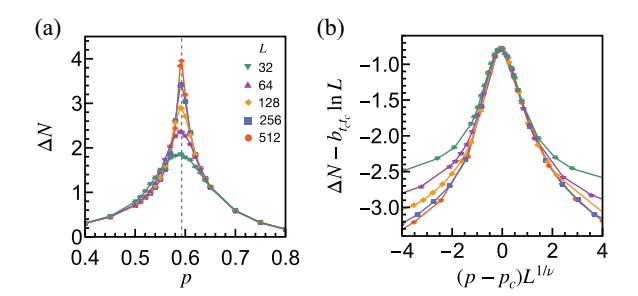


FIG. 4. (a) Corner contribution of a diagonal line (line 5) for site percolation as the occupation probability p is varied in systems of linear size L. A sharp peak is observed at the critical occupation probability  $p_c$  (dashed line). (b) Rescaling the points in (a) results in data collapse in the vicinity of the critical point with  $\nu = 4/3$ .

so at sharper angles, making the nonlinear correction easy to detect even in small systems or in the presence of noise or other statistical limitations.

#### VI. DISCUSSION

We have shown that the critical corner contribution of line segments in 2d percolation can be predicted using ideas from conformal field theory and that results in 2d and 3d can be determined numerically to high precision, making it possible to locate the critical point and extract universal information about the system from cluster counts along line segments. Although our results are presented for percolation, which is the  $Q \rightarrow 1$  limit of the Q-state Potts model, similar logarithmic terms are expected to exist for other (not necessary integer) values of Q, such as for the Ising model with Q=2, even in the presence of disorder [17], as long as the transition is continuous [14]. Techniques from conformal field theory are expected to give the correct analytic formulas also in these cases, at least for Fortuin-Kasteleyn clusters [35], as explored in 2d for lines 1 and 2 in Ref. [14]. Cluster tomography could also be explored for percolation in higher dimensions, as well as in the mean-field limit, although there are clearly no corner contributions on the Bethe lattice. In general, for higher dimensional systems, or systems lacking conformal invariance, the angledependence could be nontrivial, meaning that different configurations of cluster tomography could unveil distinct universal information.

Our results readily provide the universal term of skeletal entanglement in the critical bond-diluted transverse-field Ising model [16,36]. In this application, the natural quantity to study is the number of *crossed* clusters, where only those clusters contribute that are not fully contained by the line. Our numerical findings confirm the expectation that this difference in the definition is irrelevant at the critical point, therefore yielding the same asymptotic behavior in the quantum model.

In other cluster-based systems, including experimental realizations, it may not be possible to implement changes in the boundary conditions. As such, one or both numerical cancellation techniques may not apply. However, in many such cases the nonlinear correction may still be measured to high precision. In other cases, the nonlinear term can be accessed through comparison of direct measurements of

 $N(\ell)$  at different system sizes, which leads to cancellation of the linear term *on average*. We examine these cases in Fig. S5 of the Supplemental Material [31], demonstrating that the presence of a nonlinear corner contribution and the corresponding b exponent can be determined even without the advanced cancellation techniques, suggesting applicability of this methodology in a broad range of cluster-based systems.

Code to generate the nonlinear contribution to the cluster number count for the ten line configurations in 2d is available online [37].

#### **ACKNOWLEDGMENTS**

We thank W. Witczak-Krempa for helpful discussions. We would like to acknowledge the WCAS Summer Grant Award from the Weinberg College Baker Program in Undergraduate Research at Northwestern University. This work was supported by the National Science Foundation under Grant No. PHY-2310706 of the QIS program in the Division of Physics. This research was supported in part through the computational resources and staff contributions provided for the Quest high performance computing facility at Northwestern University which is jointly supported by the Office of the Provost, the Office for Research, and Northwestern University Information Technology.

### APPENDIX A: ANALYTIC ARGUMENTS

Bond percolation can be considered as the  $Q \to 1$  limit of the Q-state Potts model [38], defined on a lattice with sites i = 1, 2, ..., n and m nearest neighbor bonds. The partition sum of the Potts model is given by

$$Z(Q) = \sum_{s} \prod_{\langle ij \rangle} \exp\left(K\delta_{s_i, s_j}\right),\tag{A1}$$

where  $\delta_{s_i,s_j}$  is the Kronecker symbol and K is the reduced coupling, which is the ratio of the pair interaction and the temperature. Using the identity  $\exp(K\delta_{s_i,s_j}) = 1 + \frac{p}{1-p}\delta_{s_i,s_j}$  with  $p = 1 - e^{-K}$ , the sum of products in Z is written in terms of the so-called Fortuin-Kasteleyn clusters [35], denoted by F. In F an edge of the lattice i,j is occupied if a factor  $\frac{p}{1-p}\delta_{s_i,s_j}$  is present and if the spins exist in the same state within any connected cluster. Up to an irrelevant prefactor, this leads to

$$Z(Q) \sim \sum_{F} Q^{N_{\text{tot}}(F)} p^{M(F)} (1-p)^{m-M(F)}.$$
 (A2)

For a given element of F there are  $N_{\text{tot}}(F) \leq n$  connected components and  $M(F) \leq m$  occupied bonds. The mean total number of clusters is then given by

$$\langle N_{\text{tot}} \rangle = Q \frac{\partial \ln Z(Q)}{\partial Q}.$$
 (A3)

If we fix all spins on a one-dimensional contour  $\Gamma$  (in state 1, say), but leave the couplings unchanged, this relation is modified as

$$\langle N_{\text{tot}} - N_{\Gamma} \rangle = Q \frac{\partial \ln Z_{\Gamma}(Q)}{\partial Q}.$$
 (A4)

At the critical point,  $p = p_c$ , we can write [13]

$$\ln Z(Q) - \ln Z_{\Gamma}(Q) \sim f_{\rm e}(Q) L_{\Gamma} + f_{\rm c}(Q), \tag{A5}$$

where  $L_{\Gamma}$  is the linear extension of  $\Gamma$ ,  $f_{\rm e}$  is the edge freeenergy density, which is a nonuniversal quantity, and the term  $f_{\rm c}(Q)$  originates from the corners (or endpoints) of  $\Gamma$  and is known as the *corner contribution* to the free-energy, which is expected to be universal. The corner contribution to the free energy can be expressed as [27–29]

$$f_c(Q) = \left(c(Q)A_{\Gamma} + \frac{\pi}{\omega_{\Gamma}}h(Q)\right)\ln L_{\Gamma}.$$
 (A6)

The first term is the Cardy-Peschel term [27], which receives contributions from each  $\gamma_k$  corner of  $\Gamma$ , considering both the interior and exterior sides of the contour. Here c(Q) is the central charge of the Q-state Potts model, and  $A_{\Gamma}$  is a purely geometric factor that is the same for all values of Q and emerges from the angles  $\gamma_k$  as

$$A_{\Gamma} = \sum_{k} A_{\gamma_k} = \sum_{k} \frac{1}{24} \left( \frac{\gamma_k}{\pi} - \frac{\pi}{\gamma_k} \right). \tag{A7}$$

The second term in Eq. (A6) is present each time there are different boundary conditions along the contour on either side of the corner, such as a change between fixed and free boundary conditions when a measuring contour touches a free surface. The term h(Q) is the scaling dimension of the boundary condition changing operator and  $\omega_{\Gamma}$  includes the corner angle(s) at the location of the boundary condition change.

In this paper, we focus on a line segment of length  $L_{\Gamma} = \ell$  and determine the corner contribution to the cluster number count. Using Eqs. (A3) and (A4) we can write

$$N(\ell) = Q \frac{df_{\rm e}(Q)}{dQ} \ell + Q \frac{df_{\rm c}(Q)}{dQ} \equiv a\ell + b \ln \ell, \qquad (A8)$$

with b being the cluster count exponent. Percolation corresponds to  $Q \to 1$ , so using the parametrizations c(k) = 1 - 6/[k(k+1)] and  $\sqrt{Q} = 2\cos\left(\frac{\pi}{k+1}\right)$  [39] gives  $c'(1) = 5\sqrt{3}/(4\pi)$ , where prime notation indicates a derivative with respect to Q. Additionally, changing the boundary condition from fixed along the line segment to free along a boundary gives  $h'(1) = \sqrt{3}/(8\pi)$  [32]. We conjecture that b receives contributions from linear combinations of  $B(\gamma_k) = c'(1)A_{\gamma_k}$  and  $S(\gamma) = h'(1)\pi/\gamma$ , corresponding to Eqs. (2) and (3) of the main text, depending on the endpoint types (surface, bulk, or traversing) of the line segment of interest, as discussed in the main text.

# APPENDIX B: RELATION BETWEEN CLUSTER SHAPE AND b

For a system with PBC, the gap-size statistics n(s) considers the distance  $s = \min[x_{i+1} - x_i, L - (x_{i+1} - x_i)]$  between successive occurrences  $x_i$  of a given cluster along a line through a clustered system of size L, quantifying the frequency with which a gap of size s occurs. For a convex simply connected cluster, there are no gaps above size 1. In contrast, a broad gap-size statistics implies concavity in the shape of the clusters at all scales. Note that the gap-size statistics captures higher order correlations in the structure, as a gap of size s

requires not only that sites  $x_{i+1}$  and  $x_i$  are part of the cluster, but also that all s-1 sites between them are not part of the same cluster. For lines 1 and 2, the gap-size statistics is related to the corner contribution along a line segment of length  $\ell \leq L/2$  with PBC through [36]

$$C(\ell) = \frac{1}{2L} \sum_{i=1}^{\ell} \sum_{s=i}^{L/2} n(s).$$
 (B1)

In all previously studied cases, at criticality  $n(s) \sim s^{-\zeta}$  with  $\zeta = 2$  [14,16,36]. After approximating the sum as an integral,

- this results in the logarithmic corner contribution to the cluster number count in Eq. (1).
- As discussed in the main text, measures of cluster tomography on the surface of a 3d cube at criticality suggest b = 0, indicating that n(s) might decay faster in these cases. Exploring n(s) of line segments on the face of a cube for site and bond percolation, shown in Fig. S4 of the Supplemental Material [31], we find universal behavior with exponent  $\zeta = 2.30(5)$ . This further confirms the vanishing cluster count exponent in this case and provides an example of a critical system for which  $\zeta \neq 2$ .
- S. V. Komogortsev, R. S. Iskhakov, and V. A. Felâk, Fractal dimension effect on the magnetization curves of exchangecoupled clusters of magnetic nanoparticles, J. Exp. Theor. Phys. 128, 754 (2019).
- [2] J. Tailleur and M. E. Cates, Statistical mechanics of interacting run-and-tumble bacteria, Phys. Rev. Lett. 100, 218103 (2008).
- [3] I. Buttinoni, J. Bialké, F. Kümmel, H. Löwen, C. Bechinger, and T. Speck, Dynamical clustering and phase separation in suspensions of self-propelled colloidal particles, Phys. Rev. Lett. 110, 238301 (2013).
- [4] J. Palacci, S. Sacanna, A. P. Steinberg, D. J. Pine, and P. M. Chaikin, Living crystals of light-activated colloidal surfers, Science 339, 936 (2013).
- [5] A. Be'er, B. Ilkanaiv, R. Gross, D. B. Kearns, S. Heidenreich, M. Baer, and G. Ariel, A phase diagram for bacterial swarming, Commun. Phys. 3, 66 (2020).
- [6] G. W. Swart, Activated leukocyte cell adhesion molecule (CD166/ALCAM): Developmental and mechanistic aspects of cell clustering and cell migration, Eur. J. Cell Biol. 81, 313 (2002).
- [7] H. Guo, I. Lee, M. Kamar, S. K. Akiyama, and M. Pierce, Aberrant N-glycosylation of β1 integrin causes reduced α5β1 integrin clustering and stimulates cell migration, Cancer Res. 62, 6837 (2002), https://aacrjournals.org/cancerres/article-pdf/ 62/23/6837/2499428/ch2302006837.pdf.
- [8] T. Vicsek, A. Czirók, E. Ben-Jacob, I. Cohen, and O. Shochet, Novel type of phase transition in a system of self-driven particles, Phys. Rev. Lett. 75, 1226 (1995).
- [9] A. Cavagna and I. Giardina, Bird flocks as condensed matter, Annu. Rev. Condens. Matter Phys. 5, 183 (2014).
- [10] Y. Katz, K. Tunstrøm, C. C. Ioannou, C. Huepe, and I. D. Couzin, Inferring the structure and dynamics of interactions in schooling fish, Proc. Natl. Acad. Sci. USA 108, 18720 (2011).
- [11] D. M. Gordon, The ecology of collective behavior, PLoS Biol. **12**, e1001805 (2014).
- [12] R. Yu, H. Saleur, and S. Haas, Entanglement entropy in the two-dimensional random transverse field Ising model, Phys. Rev. B 77, 140402(R) (2008).
- [13] I. A. Kovács, F. Iglói, and J. Cardy, Corner contribution to percolation cluster numbers, Phys. Rev. B 86, 214203 (2012).
- [14] I. A. Kovács, E. M. Elçi, M. Weigel, and F. Iglói, Corner contribution to cluster numbers in the Potts model, Phys. Rev. B 89, 064421 (2014).

- [15] C. Berthiere and W. Witczak-Krempa, Entanglement of skeletal regions, Phys. Rev. Lett. **128**, 240502 (2022).
- [16] I. A. Kovács and F. Iglói, Corner contribution to percolation cluster numbers in three dimensions, Phys. Rev. B 89, 174202 (2014).
- [17] I. A. Kovács, J.-C. A. d'Auriac, and F. Iglói, Excess entropy and central charge of the two-dimensional random-bond Potts model in the large-Q limit, J. Stat. Mech. (2014) P09019.
- [18] W. Witczak-Krempa, Entanglement susceptibilities and universal geometric entanglement entropy, Phys. Rev. B 99, 075138 (2019).
- [19] D. Stauffer and A. Aharony, *Introduction to Percolation Theory* (Taylor & Francis, London, 1992).
- [20] S. Smirnov, Critical percolation in the plane: conformal invariance, Cardy's formula, scaling limits, C. R. Acad. Sci. Paris Sér. I Math. 333, 239 (2001); J. Tsai, S. C. P. Yam, and W. Zhou, Conformal invariance of the exploration path in 2-d critical bond percolation in the square lattice, arXiv:1112.2017.
- [21] J. L. Cardy, Conformal invariance, in *Phase Transitions and Critical Phenomena*, edited by C. Domb and J. Lebowitz (Academic, London, 1987), Vol. 11, p. 55.
- [22] O. Schramm, Scaling limits of loop-erased random walks and uniform spanning trees, Isr. J. Math. 118, 221 (2000).
- [23] S. Smirnov and W. Werner, Critical exponents for two-dimensional percolation, Math. Res. Lett. 8, 729 (2001).
- [24] P. Kleban and R. M. Ziff, Exact results at the two-dimensional percolation point, Phys. Rev. B 57, R8075 (1998).
- [25] V. Dotsenko and V. Fateev, Conformal algebra and multipoint correlation functions in 2D statistical models, Nucl. Phys. B 240, 312 (1984).
- [26] J. L. Cardy, Critical percolation in finite geometries, J. Phys. A 25, L201 (1992).
- [27] J. L. Cardy and I. Peschel, Finite-size dependence of the free energy in two-dimensional critical systems, Nucl. Phys. B 300, 377 (1988).
- [28] J. L. Cardy, Boundary conditions, fusion rules and the Verlinde formula, Nucl. Phys. B 324, 581 (1989).
- [29] J.-M. Stéphan and J. Dubail, Logarithmic corrections to the free energy from sharp corners with angle  $2\pi$ , J. Stat. Mech. (2013) P09002.
- [30] J. van den Berg and R. Conijn, The expected number of critical percolation clusters intersecting a line segment, Electron. Commun. Probab. 21, 1 (2016).
- [31] See Supplemental Material at http://link.aps.org/supplemental/ 10.1103/PhysRevResearch.5.043218 for Figs. S1–S5,

- showing schematic images of the contributions to  $T(\gamma,\omega)$ , using the boundary changing method, and 3d line configurations, and plots of the gap-size statistics for 3d surface lines, and determining b without using the geometric or boundary changing methods.
- [32] J. Cardy, Conformal invariance and percolation, arXiv:mathph/0103018.
- [33] C. D. Lorenz and R. M. Ziff, Precise determination of the bond percolation thresholds and finite-size scaling corrections for the sc, fcc, and bcc lattices, Phys. Rev. E 57, 230 (1998); Universality of the excess number of clusters and the crossing probability function in three-dimensional percolation, J. Phys. A 31, 8147 (1998).
- [34] J. Wang, Z. Zhou, W. Zhang, T. M. Garoni, and Y. Deng, Bond and site percolation in three dimensions, Phys. Rev. E 87, 052107 (2013).
- [35] P. W. Kasteleyn and C. M. Fortuin, Phase transitions in lattice systems with random local properties, J. Phys. Soc. Jpn. **26**, 11 (1969).
- [36] I. A. Kovács and F. Iglói, Universal logarithmic terms in the entanglement entropy of 2d, 3d and 4d random transverse-field Ising models, Europhys. Lett. **97**, 67009 (2012).
- [37] https://github.com/helenansell/cluster-tomography.
- [38] F. Y. Wu, The Potts model, Rev. Mod. Phys. 54, 235 (1982).
- [39] J. Cardy, SLE for theoretical physicists, Ann. Phys. (NY) **318**, 81 (2005).